Published online 29 November 2013

Nucleic Acids Research, 2014, Vol. 42, No. 4 ***2697–2707***
doi:10.1093/nar/gkt1170

Poly(A) RNA and Paip2 act as allosteric regulators of poly(A)-binding protein

Seung Hwan Lee[1], Jungsic Oh[2], Jonghyun Park[2], Ki Young Paek[3], Sangchul Rho[1], Sung Key Jang[3,4,*] and Jong–Bong Lee[1,2,*]

[1]School of Interdisciplinary Bioscience & Bioengineering, Pohang University of Science & Technology (POSTECH), Pohang 790-784, Korea, [2]Department of Physics, Pohang University of Science & Technology (POSTECH), Pohang 790-784, Korea, [3]Department of Life Sciences, Pohang University of Science & Technology (POSTECH), Pohang 790-784, Korea and [4]Division of Integrative Biosciences & Biotechnology, Pohang University of Science & Technology (POSTECH), Pohang 790-784, Korea

Received August 6, 2013; Revised October 26, 2013; Accepted October 30, 2013

ABSTRACT

When bound to the 3′ poly(A) tail of mRNA, poly(A)-binding protein (PABP) modulates mRNA translation and stability through its association with various proteins. By visualizing individual PABP molecules in real time, we found that PABP, containing four RNA recognition motifs (RRMs), adopts a conformation on poly(A) binding in which RRM1 is in proximity to RRM4. This conformational change is due to the bending of the region between RRM2 and RRM3. PABP-interacting protein 2 actively disrupts the bent structure of PABP to the extended structure, resulting in the inhibition of PABP-poly(A) binding. These results suggest that the changes in the configuration of PABP induced by interactions with various effector molecules, such as poly(A) and PABP-interacting protein 2, play pivotal roles in its function.

INTRODUCTION

Poly(A)-binding protein (PABP) is composed of an N-terminal domain that contains four distinct RNA recognition motifs (RRMs) and a C-terminal domain (PABC) that is not associated with poly(A) binding (1,2). According to the co-crystal structure of the RRM1-2 fragment (residues 1–190) bound to a polyadenylated [poly(A)] strand, RRM1 and RRM2 in tandem bind the 11-nt poly(A) sequence, establishing a linear conformation with the RNA (3). Although most proteins with two tandem RRMs joined by a short linker bind adjacent sites in the same RNA molecule, they show distinct conformations, such as the V-shape of the sex-lethal protein (4), the cleft-shape of the HuD protein (5), the loop-shape of the nucleolin protein bound to stem-looped RNA (6) and the RNA looping by PTB3-4 (7,8). Therefore, knowledge of the interaction between PABP and poly(A) will provide a better understanding of translational regulation by this prominent translational activator because the unique conformation of PABP bound to the RNA template could play an important role in determining its function, especially when it is in complex with other proteins.

Mechanistically, PABP has been suggested to augment global translation by enhancing the binding of the eIF4F complex to the cap (1,9–12) and by facilitating reuse of translation-terminated 40S subunit at the termination codon (13–15). The 3′ poly(A) RNA tail is brought close to the cap structure at the 5′ end of the mRNA through the interaction of PABP bound to poly(A) with eIF4G. These interactions form a bridge between the poly(A) and the 5′ cap structure via consecutive interactions of poly(A) PABP-eIF4G-eIF4E-5′ cap, resulting in the circularization of the mRNA (10). The augmentation of translation by PABP is modulated by PABP-interacting protein 1 (Paip1), which directly interacts with PABP (15–17). In contrast, PABP-interacting protein 2 (Paip2) is known to suppress translation by disrupting the circularization of mRNA mediated by PABP. Khaleghpour *et al.* (18) reported that Paip2 displaces PABP from poly(A) through physical contact with PABP. The PABP-interacting motif 1 in Paip2 binds to RRM2 and RRM3 of PABP, directing the dissociation of PABP from poly(A) (13). The interaction between RRM2 and Paip2 was shown to compete with eIF4G for binding to RRM2 (19). Although it has been observed that the direct interaction between Paip2 and PABP represses translation by regulating the poly(A) binding of PABP, the mechanism by which Paip2 inhibits the binding of PABP to poly(A) is poorly understood.

In this study, we visualized a single PABP molecule interacting with poly(A) and/or the PABP-interacting

*To whom correspondence should be addressed. Tel: +82 54 279 2095; Fax: +82 54 279 3099; Email: jblee@postech.ac.kr
Correspondence may also be addressed to Sung Key Jang. Tel: +82 54 279 2298; Fax: +82 54 279 8099; Email: sungkey@postech.ac.kr

proteins Paip1 and Paip2. The resulting kinetics and conformational changes of human PABP suggest that poly(A) transforms RRMs of PABP from a fluctuating conformation to a bent conformation on poly(A) binding, which stabilizes the poly(A) and PABP complex, and that Paip2 changes the bent conformation in the PABP-poly(A) complex to an extended conformation which results in the dissociation of PABP from poly(A). We propose that the bent conformation of PABP may play an important role in mRNA translation through the interactions with translation initiation factors.

MATERIALS AND METHODS

Purification of recombinant proteins

The procedures used to express and purify full-length human PABP (PABPC1) and partially truncated PABP domains have been described previously (20). We slightly modified the purification procedure for full-length PABP to achieve increased purity (>95%). Human PABP was cloned into the pET 28a expression vector using the restriction sites of NheI and BamHI for the addition of an N-terminal 6x-His tag and a C-terminal Flag tag, respectively. The proteins were overexpressed in the *Escherichia coli* strain BL21(DE3). Protein expression was induced for 24 h at 16°C by adding 1 mM IPTG (isopropyl β-D-1-thiogalactopyranoside). The cells were harvested and then resuspended in 100 ml lysis buffer [20 mM Tris–HCl (pH 8.0), 400 mM NaCl, 15% glycerol, 10 mM β-mercaptoethanol, 1% Triton X-100, 50 μg aprotinin, 50 μg antipain, 50 μg bestatin, 1 mM PMSF (phenylmethylsulfonyl fluoride)]. The lysed cells were centrifuged, and the supernatant was applied to 500 μl Ni-NTA agarose resin (QIAGEN) that was pre-equilibrated with binding buffer [20 mM Tris–HCl (pH 8.0), 400 mM NaCl, 15% glycerol, 10 mM β-mercaptoethanol, 1% Triton X-100]. After washing the column containing the Ni-NTA resin with the binding buffer, we eluted full-length PABP using a 50–200 mM gradient of imidazole in binding buffer. The eluted proteins were re-applied to anti-Flag M2 affinity resin (SIGMA ALDRICH) that was also pre-equilibrated with the same binding buffer.

The proteins were >95% pure, which was confirmed by the observation of a single band in a Coomassie-stained SDS-PAGE gel. The concentration of the purified recombinant proteins was measured using a NanoPhotometer (IMPLEN) and adjusted to <1 mg/ml to prevent self-aggregation. The imidazole and Flag peptide were eliminated by buffer exchange against a buffer containing 10 mM HEPES-KOH (pH 7.5), 250 mM KCl, 1 mM $MgCl_2$, 0.1 mM EDTA, 7 mM β-mercaptoethanol and 20% glycerol. Aliquots were stored at −80°C. The binding affinities of the recombinant proteins to the RNA constructs [DNA–RNA duplex with poly(A) tail] in the single-molecule experiments were identical to those of pure single-stranded poly(A) RNA (Supplementary Table S1).

GST-tagged human Paip1 and Paip2 from the expression vectors pGEX-KG and pGEX6P-2, respectively, were also overexpressed in the *E. coli* strain BL21(DE3). The purification procedure used for these proteins was identical to that used for PABP.

Fluorophore conjugation to RRM1-2, RRM1-2-3-4 and full-length PABP

To label a protein with Cy3-Cy5 or Cy5 via cysteine-maleimide interaction, we first obtained a cysteine-free PABP mutant. Four internal cysteine residues were substituted with serine residues by introducing point mutations and cysteine residues were inserted into the N- and C-termini of the cysteine-free mutant proteins to result in (His-tag)-(Cys)-(RRM1-2-3-4)-(Cys) and (His-tag)-(Cys)-(RRM1-2-3-4)-(PABC)-(Flag-tag) for RRM1-2-3-4 and full-length PABP, respectively. The cDNAs of the RRM truncation mutants were sub-cloned into the expression vector pET-28 a using the specific enzyme sites NheI and BamHI and then expressed in the *E. coli* BL21(DE3) strain. The mutated proteins were purified under the same conditions used for wild-type PABP. During the elution process, maleimide-fluorophores (Cy3, Cy5) were conjugated to the cysteines extended from the N and C termini of RRM1-2-3-4 in the presence of labeling buffer [50 mM Tris–HCl (pH 8.0), 300 mM NaCl]. The molar ratio of protein to Cy3 to Cy5 was 1:1:10 for the maleimide-cysteine reaction. However, for Cy5-labeled RRM1-2 and full-length PABP, a cysteine residue was inserted into the N-terminal site of the RRM1 of a cysteine-free mutant RRM1-2 and full-length PABP and Cy5-maleimide was conjugated to the cysteine of the proteins using a 10-fold molar excess of Cy5 to protein. After the samples were stringently washed to remove the non-conjugated fluorophores, the fluorophore-conjugated proteins were eluted with 200 mM imidazole. The imidazole was then eliminated by buffer exchange into storage buffer [50 mM Tris–HCl (pH 7.7), 300 mM NaCl, 20% glycerol]. Aliquots of the proteins were quickly frozen with liquid nitrogen and stored at −80°C. The poly(A) affinities of the mutant proteins were nearly identical to those of the wild-type protein (Supplementary Table S1).

Photobleaching analysis by the simultaneous excitation of Cy3 and Cy5 using 532- and 633-nm lasers indicated that 36% of fluorophore-labeled RRM1-2-3-4 contained the donor–acceptor pair. To test the specific labeling of the probes to a cysteine residue, the photobleaching steps of RRM1-2-3-4 obtained from 133 molecules bound to $poly(A)_{25}$ templates were investigated. The photobleaching steps of the donor Cy3 showed a single step of 93% and two steps of 7% but no more than two steps. The 7% two steps could have resulted from a donor–donor pair labeled on RRM1-2-3-4 or two donor only-labeled RRM1-2-3-4 proteins near the poly(A) template. The labeling efficiency for Cy5-RRM1-2 and Cy5-PABP was measured by spectrophotometry (IMPLEN) and the resulting labeling efficiency was 40 and 70%, respectively.

Poly(A) RNA constructs

We prepared PAGE or HPLC-purified DNA and RNA oligos that were modified with biotin, Dy547 and Dy649 from Thermo Fisher Scientific and IDT (Coralville, USA)

to construct the following partial duplex DNA/RNA substrates: 5′-AGU UAC AGA UUU AUG CCC poly(A)$_n$ GG/Dy547-3′ for the RNA strand and 5′-Dy649/GGG CAT AAA TCT GTA ACT/Biotin/-3′ for the DNA strand. For the experiments with fluorescently labeled RRM1-2 and full-length PABP, we used the partial duplex of 5′-AGU UAC AGA UUU AUG CCC poly(A)$_n$ GG/Dy547(null)-3′ ($n = 15$ or 25 nt) and 5′-(Cy3)-GGG CAT AAA TCT GTA ACT/Biotin/-3′. For the full-length PABP and RRM1-2-3-4 proteins containing Cy3 and Cy5, 5′-AGU UAC AGA UUU AUG CCC poly(A)$_n$ GG-3′ and 5′-Dy649/GGG CAT AAA TCT GTA ACT/Biotin/-3′ were used for the template. Partial duplex substrates that consisted of an 18-bp DNA/RNA duplex with a 5′-overhang of G-poly(A)$_n$-GG ($n = 15$, 25 or 37 nt) were prepared by annealing pairs of DNA oligos and RNA oligos at a molar ratio of 1:6 in annealing buffer [10 mM Tris–HCl (pH 7.5), 100 mM KCl, 1 mM EDTA] for a final concentration of 100 nM. The solution containing the oligos was incubated in an 80°C water bath for 5 min and was then slowly cooled down to room temperature over 3 h. The annealed substrates were stored at 4°C.

Single-molecule FRET experiments

We performed single-molecule FRET (smFRET) experiments using a prism-type total internal reflection fluorescence microscope to collect the fluorescent signals. The emission signals from the donor and acceptor were separated by a dual-channel, simultaneous imaging system (DV2, Mag Biosystems) into two channels to independently measure the donor intensity and acceptor intensity, respectively. The method used for the single-molecule time-lapse FRET experiment (21) and the sample chamber protocols, experimental procedures and data analysis (22) have been described in previous studies.

To immobilize Cy3/Cy5-labeled or wild-type PABP onto the streptavidin-conjugated quartz surface modified with Biotin-PEG, a biotinylated anti-His mouse antibody (Santa Cruz Biotechnology) was diluted to 1 nM in blocking buffer [10 mM Tris–HCl (pH 8.0), 50 mM NaCl, 0.0025% (v/v) Tween-20] and incubated in the flow chamber for 10 min. Free antibodies were removed by stringently washing with blocking buffer. After His-tagged PABP proteins (10 nM) were infused into the flow chamber coated with the anti-His antibody, the donor and acceptor signals from PABP that was bound to the surface were collected in the presence of reaction buffer [10 mM Tris–HCl (pH 8.0), 100 mM KCl] containing oxygen scavenging materials [1 mg/ml glucose oxydase, 0.4% (w/v) D-glucose, 0.04 mg/ml catalase, 2 mM Trolox]. All single-molecule experiments were carried out at 23°C (±1°C).

Data analysis

The time traces of the fluorescence intensity and FRET efficiency shown in the figures were all filtered with a forward–backward non-linear filter (23). The histograms of FRET efficiency were taken from the time trace of the FRET efficiency for 10 s before the FRET transition and for 10 s after the transition of the FRET value except the histograms in Figure 5 that were constructed from the FRET values for 3 s instead of 10 s, and the histograms in Figure 3 that were built from the FRET efficiency averaged at each trace. The density plots in Figures 2d, 2e and 4b were obtained by adding individual FRET traces in the same time scale. The FRET efficiency due to photobleaching was forced to zero. The FRET efficiency denoted in the text indicates mean and standard deviation obtained from the FRET distribution.

Measurement of the dissociation constant

In the second order chemical reaction of the receptor-ligand binding, the dissociation constant (K_d) in equilibrium is defined as

$$K_d = \frac{[R][L]}{[RL]},$$

where $[R]$, $[L]$ and $[RL]$ are the concentrations of the receptor, the ligand and the ligand-bound receptor, respectively. The probability of the receptor-ligand binding (P_{bound}) can be expressed in terms of the concentrations of free receptors $[R]$ and ligand-bound receptors $[RL]$. With the help of the relation $[RL] = [R][L]/K_d$, we arrive that

$$P_{bound} = \frac{[RL]}{[R]+[RL]} = \frac{[L]}{K_d+[L]}.$$

To obtain Figure 2c, we measured the numbers of PABP-free poly(A)$_{25}$ for $[R]$ ($E \sim 0.4$) and PABP-bound poly(A)$_{25}$ for $[RL]$ ($E \sim 0.8$) at different concentrations of PABP ($[L_{total}]$) for $[L]$ ($= [L_{total}]-[RL]$). We assumed that $[L] \sim [L_{total}]$, as the number of the immobilized poly(A)$_{25}$ is extremely smaller than the free ligand in the solution ($[L] >> [RL]$).

RESULTS

Single-molecule assay to study poly(A) binding by PABP

The RRM1 and RRM2 domains of PABP, arranged in tandem, stretch the poly(A) strand through contacts to sequential nucleotides (3) (Figure 1a). The lengthening of the poly(A) strand allows us to use single-molecule fluorescence resonance energy transfer (smFRET) to investigate the real-time dynamics of an individual RRM1-2 fragment binding to a poly(A) strand. A partial duplex substrate that consisted of an 18 bp DNA–RNA duplex with a 3′ adenosine RNA tail [poly(A)$_n$] of varying lengths ($n = 15$, 25 or 37 nucleotides) was prepared for the smFRET experiments. The lengths of 11 and 25 nucleotides cover RRM1-2 and full-length PABP, respectively (24–26). A biotin molecule attached to the 3′ end of the DNA in the partial duplex template was anchored to a quartz slide that was functionalized with polyethylene glycol (PEG)-biotin through a biotin-streptavidin interaction (Figure 1b). A FRET donor-Dy547 and a FRET acceptor-Dy649 were covalently attached to the 5′ end of the DNA and the 3′ end of the RNA, respectively (Figure 1b).

Figure 1c shows representative time traces of the donor–acceptor intensity and its resulting FRET efficiency

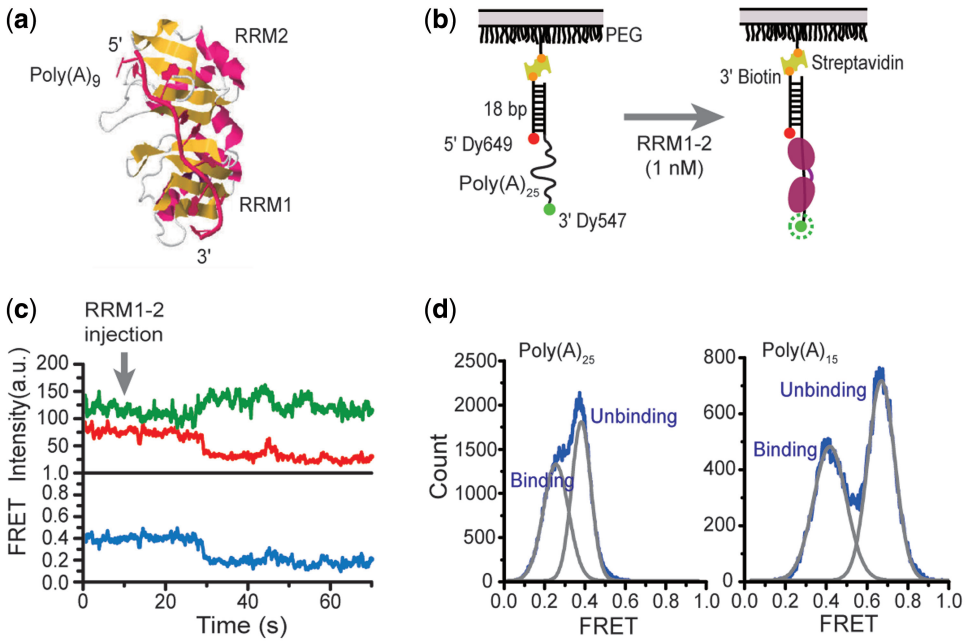

Figure 1. Single-molecule FRET for poly(A) binding by the RRM1-2 fragment. (**a**) The crystal structure of the RRM1-2 fragment (residues 1–190; PDB: 1cvj). The RRM1 and RRM2 are connected by the 9-residue linker. The remaining RRMs in full-length PABP are connected by 14 and 26-residue linkers, and PABC is connected to RRM4 by the 178-residue proline-rich linker. (**b**) Schematic representation of the poly(A)$_{25}$ template that bears a donor Dy547 and an acceptor Dy649. (**c**) Representative traces showing the donor–acceptor intensity and the resulting FRET values in the presence of 1 nM RRM1-2. (**d**) Histograms of the FRET values obtained from poly(A)$_{25}$ (N = 131) and poly(A)$_{15}$ (N = 100) molecules in the presence of RRM1-2, respectively.

(E). RRM1-2 fragments (1 nM) in 100 mM NaCl were infused at 10 s into a flow chamber in which poly(A)$_{25}$ templates had been immobilized. Twenty seconds after the injection, the acceptor signal decreased and the donor signal increased. These anticorrelated signals resulted in the transition of the FRET efficiency from 0.4 to 0.2. The FRET efficiency for 10 s before and 10 s after the FRET transition showed a double Gaussian distribution with two peaks, 0.38 ± 0.09 (mean ± s.d.) and 0.26 ± 0.13. The lower FRET efficiency appears to be the result of poly(A) binding to RRM1-2 (N = 131; Figure 1d). The FRET value associated with the binding of RRM1-2 to poly(A)$_{15}$ was 0.43 ± 0.17, and the unbound poly(A)$_{15}$ displayed a FRET efficiency of 0.67 ± 0.13 (N = 100; Figure 1d; Supplementary Figure S1). We confirmed that the binding of PABP and its fragments to the poly(A)$_{25}$ template did not result in fluorescence enhancement or fluctuation (Supplementary Figure S2). Thus, the measured FRET values indicate that RRM1-2 extends poly(A) from a probable helical structure (27) and that these two RRMs bind poly(A) in a continuous fashion, which is consistent with the co-crystal structure of RRM1-2 and poly(A) (3).

Full-length PABP bends poly(A)

To explore the conformation of RRMs in full-length PABP, which is currently unknown, we examined the conformation of the poly(A) bound to PABP. Representative traces of the donor–acceptor intensity and the resulting FRET efficiency (Figure 2a) for full-length PABP binding to poly(A)$_{25}$ show that the fluorescent signal of the donor abruptly decreased and that the acceptor signal simultaneously increased at a certain time after the injection of PABP (10 s), which resulted in a transition to the high FRET efficiency of 0.8 due to the poly(A) binding by PABP. This finding stands in direct contrast to the transition to a lower FRET efficiency that was observed for the binding of poly(A)$_{25}$ by RRM1-2.

Forty-seven percent of the events of full-length PABP binding resulted in the sudden transition to a high FRET efficiency without any detectable intermediate states within the 50-ms time resolution (Figure 2a left). However, 28% of the events appeared to contain a transitional low FRET of 0.2 before the high FRET of 0.8 (Figure 2a middle). The remaining 25% of the events displayed intermediate FRET values between E = 0.4 and E = 0.8 (Figure 2a right). This observation suggests that RRM1-2 or RRMs other than RRM1-2 bind to poly(A) before the full-length PABP is associated with the template. However, all of the binding events of full-length PABP eventually resulted in a steady fluorescence emission from the donor–acceptor pair with a high FRET value (0.81 ± 0.13; N = 160; Figure 2b orange line). We also measured the FRET efficiency with poly(A)$_{37}$. The resulting FRET value (0.62 ± 0.13; N = 134) was lower than that for poly(A)$_{25}$ (Figure 2b blue line). This result differs from the nearly constant FRET at various lengths of the RNA for PTB3-4 that forms an unbound RNA loop between the RRMs bound to the RNA ends (28). Interestingly, the portion of the events showing the intermediate FRET states significantly decreased at the longer poly(A) (Supplementary Figure S3). To determine the dissociation constant (K_d) of PABP to poly(A)$_{25}$, we investigated the fraction of poly(A)$_{25}$ bound by

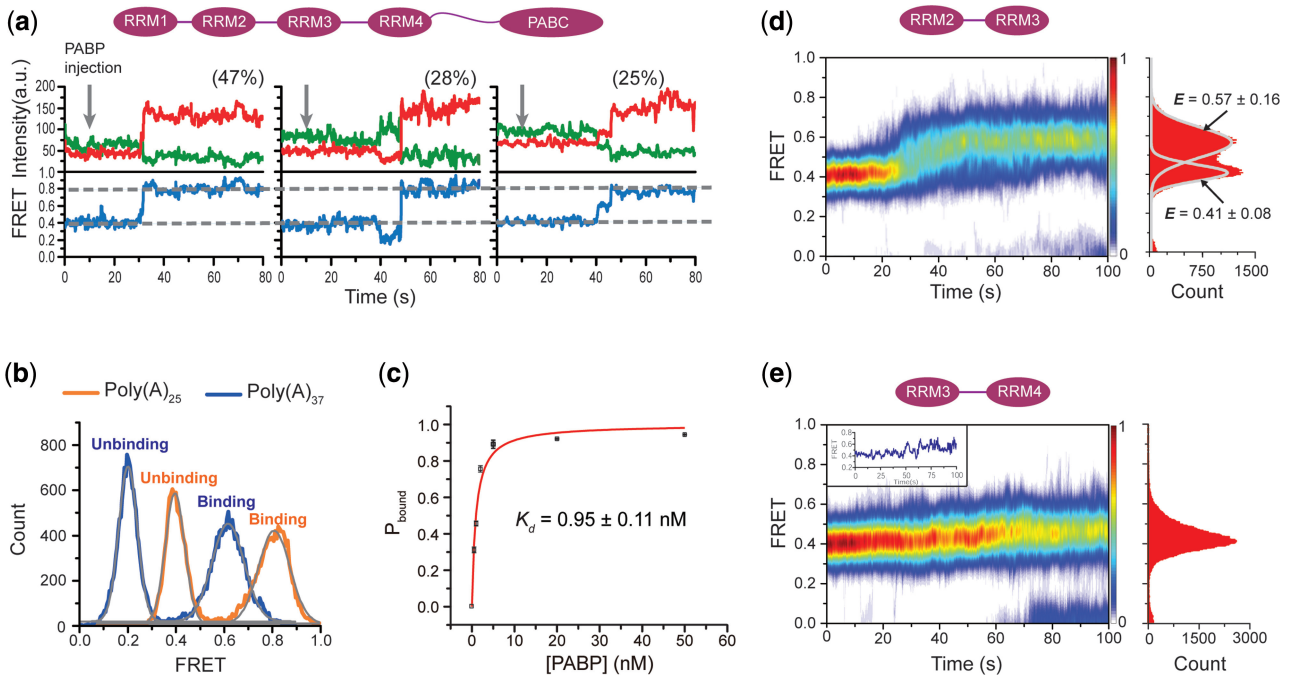

Figure 2. FRET analysis of poly(A) binding by full-length PABP, RRM2-3 and RRM3-4. (**a**) Three representative traces of the donor–acceptor intensity and FRET efficiency when full-length PABP binds to poly(A)$_{25}$ labeled with a Dy547-Dy649 pair. (**b**) The distribution of FRET efficiency observed during the association of full-length PABP with poly(A)$_{25}$ and poly(A)$_{37}$. (**c**) P_{bound} indicates that the ratio of the number of PABP-bound poly(A)$_{25}$ ($E \sim 0.8$) to the total number of PABP-unbound ($E \sim 0.4$) and PABP-bound poly(A)$_{25}$. (**d** and **e**) Density plots of the FRET efficiency when RRM2-3 ($N = 108$) and RRM3–4 ($N = 103$; inset: a representative FRET trace) bind to poly(A)$_{25}$, respectively. The plots were produced by superimposing the individual FRET traces after synchronizing all of the traces to the injection time. The histograms were taken from the FRET values in the density plots.

PABP (P_{bound}) at various concentrations of PABP (Figure 2c; 'MATERIALS and METHODS'). The resulting K_d was 0.95 ± 0.11 nM (mean ± s.e.), which nearly identical to that measured in the bulk (Supplementary Table S1). Taken as a whole, these results suggest that the binding of full-length PABP causes the donor to be in proximity to the acceptor by bending the RNA and that each RRM consecutively binds adjacent sites on the RNA.

To test which RRM domains contribute to high FRET efficiency that occurs on the binding of poly(A) by RRM1-2-3-4, we investigated the FRET values of PABP fragments that were bound to poly(A)$_{25}$. The density plot of the FRET efficiency obtained from the poly(A)$_{25}$ binding events ($N = 108$) using 1 nM RRM2-3 (residues 96–264) displays two-peaked distribution of FRET efficiency when RRM2-3 was bound to poly(A) (Figure 2d; 0 s injection). The histogram of the FRET efficiency in the density plot shows a FRET transition from a middle FRET peak (0.41 ± 0.08) to a high FRET peak (0.57 ± 0.16), which results from poly(A)$_{25}$ binding by RRM2-3 (Supplementary Figure S4). This result suggests that the region between RRM2 and RRM3 bends the poly(A). On the other hand, the binding event of 1 nM RRM3-4 (residues 179–367) displayed a FRET fluctuation (Figure 2e inset), which is likely to be resulted from the fluctuation of the linker between the RRMs when RRM3-4 bound to poly(A) (0 s injection; $N = 103$; Figure 2e). This measurement suggests that the binding of RRM3-4 also bends the poly(A) strand slightly. Taken together, these observations support our conclusion that the region between RRM2 and RRM3 primarily contributes to the bent conformation of RRM1-2-3-4 and the region between RRM3 and RRM4 partially contributes to the bent conformation.

Unidirectional binding of PABP to poly(A)

The poly(A)-binding order of the RRM domains is topologically important because each RRM and C-terminal domain of PABP interacts with other proteins that are spatially distributed on mRNA (1,29–32). To examine the FRET efficiency between an acceptor attached to N-terminus of RRM1 and a donor Dy547 attached to the 3′ end of the poly(A)$_{15}$, a Cy5 acceptor was covalently attached to a cysteine residue that had been inserted into an N-terminal site of RRM1 within a cysteine-free mutant RRM1-2 (C58S, C143S) (Figure 1a). If RRM1 and RRM2 bind to poly(A)$_{15}$ in a random direction, the histogram of the FRET is expected to display a Gaussian distribution with two peaks of high FRET efficiency that occur when RRM1 is close to the 3′ end of the poly(A)$_{15}$ and one peak of a lower FRET efficiency that results from a reversed direction of RRM1-2 binding. The peaks of the FRET efficiency can be separated by a dimension (4.7 nm) of RRM1-2 bound to poly(A)$_{15}$ (3). The histogram of the FRET efficiency was constructed from the averaged FRET values of single binding traces of individual RRM1-2 molecules bound to poly(A)$_{15}$, and it shows a narrow distribution with a peak of 0.88 ± 0.13 when RRM1-2 binds to poly(A)$_{15}$ (Figure 3a; $N = 144$). However, the high-efficiency FRET state shifted to an

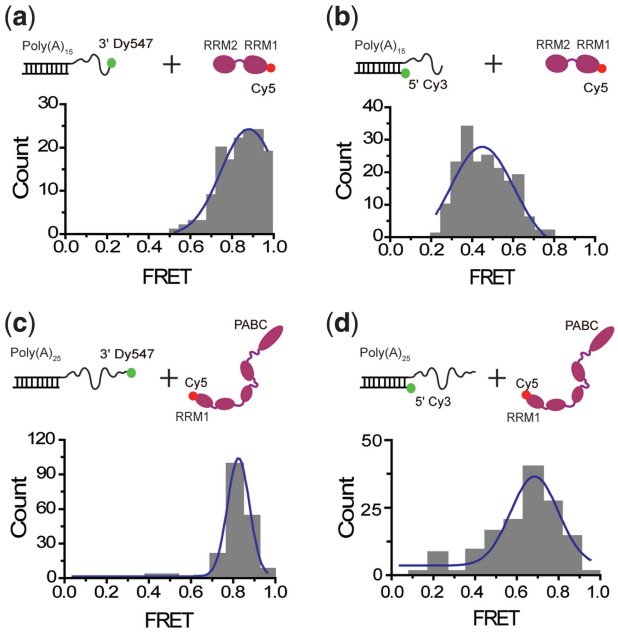

Figure 3. The RRMs are unidirectionally arranged from the 3′ end to the 5′ end of poly(A). (**a**) A narrow distribution with a peak of 0.88 ± 0.13 was observed when RRM1-2 bound to $poly(A)_{15}$ ($N = 144$). (**b**) The high-efficiency FRET state shifted to an intermediate FRET range (0.45 ± 0.16; $N = 204$) when the donor-Cy3 was attached to the 5′ end of the DNA at the junction of the DNA–RNA duplex. (**c**) A distribution of FRET efficiency between Cy5-PABP and the Dy547-3′ end of $poly(A)_{25}$ at the 3′ end (0.82 ± 0.05; $N = 194$) (**d**) A broad FRET distribution between Cy5-PABP binding and the Cy3 at the 5′ end of the DNA associated with the $poly(A)_{25}$ template (0.69 ± 0.11; $N = 137$).

intermediate FRET range (0.45 ± 0.16; $N = 204$) when the donor-Cy3 was attached to the 5′ end of the DNA at the junction of the DNA–RNA duplex (Figure 3b). These observations are interpreted to mean that the RRM1 and RRM2 domains in tandem are unidirectionally aligned 3′ to 5′ along the poly(A) when PABP binds to the poly(A), which is consistent with the X-ray crystallographic data from the RRM1–2 fragment bound to poly(A) (3).

To confirm the directionality of full-length PABP binding to poly(A), we carried out similar FRET experiments with Dy547-labeled $poly(A)_{25}$ at the 3′ end and Cy5-labeled full-length PABP at N-terminus. The resulting FRET shows a narrow distribution with a peak of 0.82 ± 0.05 ($N = 194$; Figure 3c). However, when the donor-Cy3 was attached to the 5′ end of the DNA at the junction of the DNA–RNA duplex, the high FRET distribution appeared to be broad with a peak of the FRET (0.69 ± 0.11; $N = 137$; Figure 3d). The FRET state is most likely to be generated by the bent conformation of full-length PABP on poly(A). Taken together, we conclude that the full-length PABP from RRM1 to RRM4 in sequential order is unidirectionally aligned in the 3′ to 5′ direction on poly(A) RNA.

PABP tightly bound to poly(A), and Paip2 facilitates dissociation of PABP from poly(A)

The strong binding of human full-length PABP to poly(A) (dissociation constant = 0.6 nM (20); Supplementary Table S1) led us to use a time-lapse FRET experiment to examine the kinetics of full-length PABP on $poly(A)_{25}$. For the time-lapse experiment, fluorescent signals were collected over a 50-ms time resolution (excitation-on) and a 1.95-s time interval (excitation-off) for 2000 s (Figure 4a). The pH (8.0) of the buffered solution containing oxygen scavenging materials in the sample chamber was not significantly altered in this time scale (33). The high FRET state that resulted from the binding of poly(A) by full-length PABP was steadily maintained for 1700 s (from 300 to 2000 s) after infusion at 250 s with 5 nM PABP. Figure 4b shows the density plot of the FRET efficiency in the FRET time traces of 120 full-length PABP molecules bound to poly(A), for which all data were synchronized from 0 to 2000 s. Most of the PABP proteins attained the stable FRET state with $E = 0.79$. Seventy percent of the events remained in the high FRET state until 2000 s, and the remaining 30% showed the dissociation of PABP from the poly(A) or photobleaching of the acceptor. This observation indicates that the four RRMs of PABP stably bind to $poly(A)_{25}$ for >10 min.

To address how PABP tightly bound to poly(A) is dissociated from the RNA by Paip2, GST-Paip2 (85 nM) was infused into a sample chamber in which full-length PABP proteins were pre-assembled with $poly(A)_{25}$ (Figure 4c cartoon). Shortly after the injection of Paip2 (20 s), the FRET signal of 0.8 from the $poly(A)_{25}$ bound by PABP abruptly decreased to $E = 0.4$, which is identical to the FRET value of the PABP-unbound state ($N = 570$) (Figure 4c). This result suggests that the abrupt FRET change from $E = 0.8$ to $E = 0.4$ is due to the instantaneous dissociation of PABP from the poly(A) RNA with the help of Paip2 within the time resolution of 50 ms. However, we have also observed that the FRET efficiency gradually decreased to $E = 0.4$ through the various intermediate FRET states (Supplementary Figure S5). As a control, we confirmed that the GST fragment alone did not dissociate PABP bound to poly(A) (Supplementary Figure S6). The duration (τ_{ass}) from the injection of Paip2 to the FRET change decreased as the increase of the concentration of Paip2 (Figure 4d). The resulting association rate (K_{ass}) obtained from the slope was $1.53 \times 10^5\,M^{-1}\,s^{-1}$ (Figure 4d). Taken together, we conclude that the binding of Paip2 to PABP associated with poly(A) results in the quick dissociation of all of the RRMs of PABP from poly(A), but a small portion of these dissociations occurs through the slow and sequential dissociation of each RRM from poly(A) before PABP eventually undergoes a complete dissociation from poly(A).

Direct observation of the conformational changes of the RRMs

To further explore the conformation of PABP, a donor (Cy3)–acceptor (Cy5) pair was conjugated to cysteine residues that were inserted into the N-terminus of RRM1 and the C-terminus of RRM4 in an engineered RRM1-2-3-4 with cysteine-to-serine substitutions, which has a truncation of the PABC including the linker for RRM4 (Figure 5a; 'MATERIALS and METHODS';

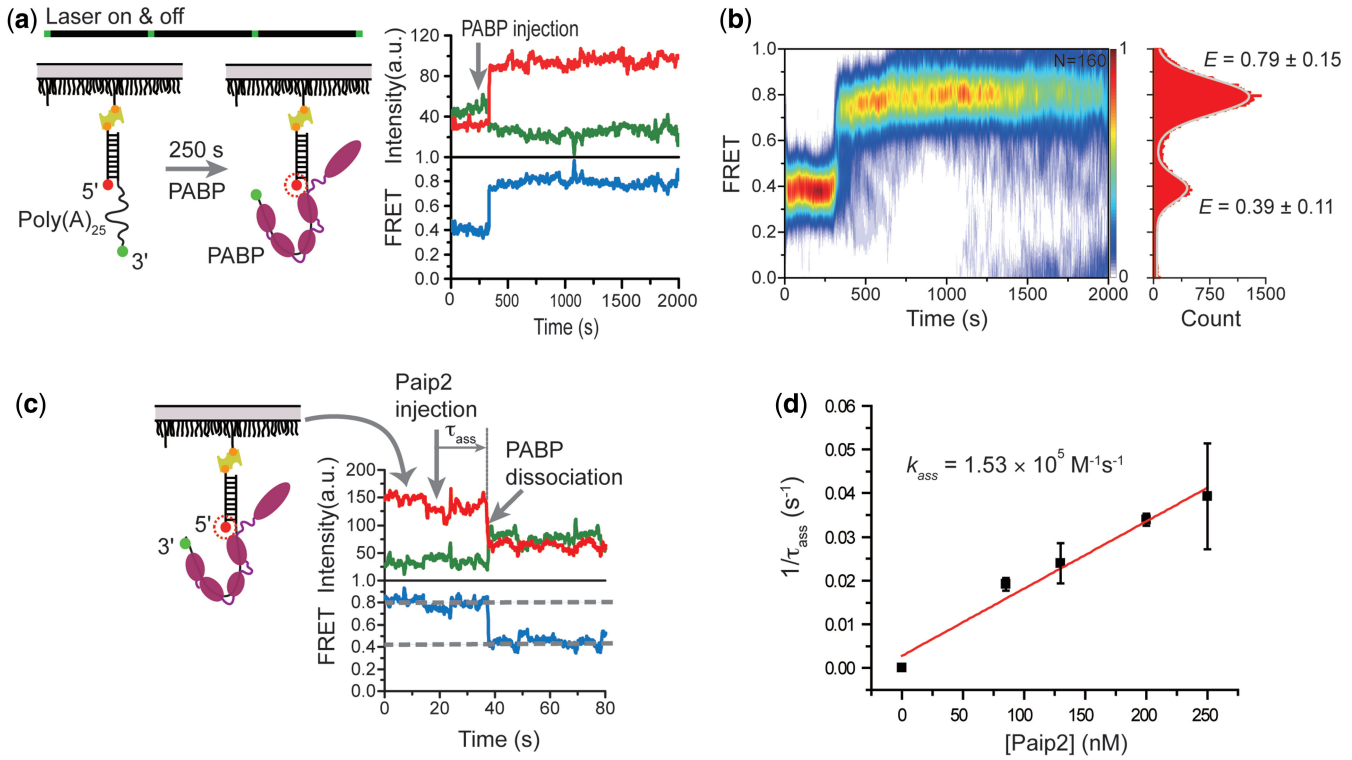

Figure 4. Paip2 dissociates PABP from its tight complex with poly(A). (**a**) Representative time traces of a time-lapse experiment showing PABP binding to poly(A)$_{25}$. In this experiment, 5 nM of full-length PABP was injected into the flow chamber at 250 s. (**b**) The density plot was generated using the FRET efficiency obtained from 160 time traces after synchronizing all of the data from 0 to 2000 s. (**c**) A representative time trace for full-length PABP that is pre-assembled with poly(A)$_{25}$ in the presence of the Paip2 proteins. τ_{ass} indicates the duration of time from the injection of Paip2 to the first FRET change. (**d**) $1/\tau_{ass}$ of Paip2 on PABP bound to poly(A) as a function of the Paip2 concentration.

Supplementary Figures S7 and S8). The RRM1-2-3-4 showed poly(A)-binding activity that was nearly identical to wild-type full-length PABP (Supplementary Table S1). Another fluorophore, Dy649, was attached to the 5′ end of the DNA oligo at the junction of the DNA–RNA duplex of the poly(A)$_{25}$ template and was used to distinguish the PABP bound to poly(A) from the PABP non-specifically bound to the quartz surface (Figure 5b cartoon). After the Dy649 on the template was photobleached with a strong laser illumination, fluorophore-labeled RRM1-2-3-4 proteins (1 nM) were injected into the flow chamber. The RRM1-2-3-4 (N = 123) showed a steadily high FRET efficiency as long as it was bound to the poly(A)$_{25}$ template (0.85 ± 0.09; Figure 5b; Supplementary Figure S9). This finding is another strong piece of evidence for the bent structure of PABP associated with poly(A).

The conformation of the four RRMs in the absence of poly(A) was analyzed by observing the mutant RRM1-2-3-4, which was immobilized on the quartz surface through the interaction between the polyhistidine (6 x-His) tag introduced at the N-terminus of RRM1-2-3-4 and the anti-6 x-His antibody bound to the surface (Figure 5a; 'MATERIALS and METHODS'). The number of fluorescent spots from the 6 x-His-tagged RRM1-2-3-4 labeled with a donor–acceptor pair when the surface of the flow chamber was coated with the anti-6 x-His antibody was 25-fold more than that when the surface of the flow chamber that was coated with the anti-Flag antibody (34–36) (Supplementary Figure S10). Therefore, the non-specific binding of RRM1-2-3-4 to the surface was negligibly contributed to the analysis of FRET signals for the conformation of RRM1-2-3-4. RRM1-2-3-4 in the absence of poly(A) displayed a broad distribution of FRET efficiency (N = 217; Figure 5c) that resulted from the fluctuation of flexible linkers between the RRMs (Supplementary Figure S11a). When 25-nt poly(A) molecules (500 nM) were infused into a chamber containing immobilized RRM1-2-3-4, the fluctuating anticorrelated emission signals of the donor–acceptor pair appeared steady with a high FRET efficiency ($E \sim 0.8$) (Supplementary Figure S11b). The resulting FRET distribution of RRM1-2-3-4 obtained from 103 molecules showed a Gaussian peak of 0.73 ± 0.13 (Figure 5d), which was separated by 0.12 from the FRET distribution in Figure 5b. The FRET shift may result from the different binding condition of RRM1-2-3-4 to poly(A). Taken together, these results strongly support that poly(A) binding to RRM1-2-3-4 shifts the disordered configuration of RRM1-2-3-4 to a steady and bent conformation.

To directly observe the conformational change of RRM1-2-3-4 that occurs on Paip2 binding, the fluorescence signals from RRM1-2-3-4 in the presence of poly(A) and Paip2 were analyzed. The high FRET efficiency ($E \sim 0.8$) induced by binding to poly(A) was significantly reduced, and a much lower FRET state appeared (Supplementary Figure S11c), indicating that Paip2 forms

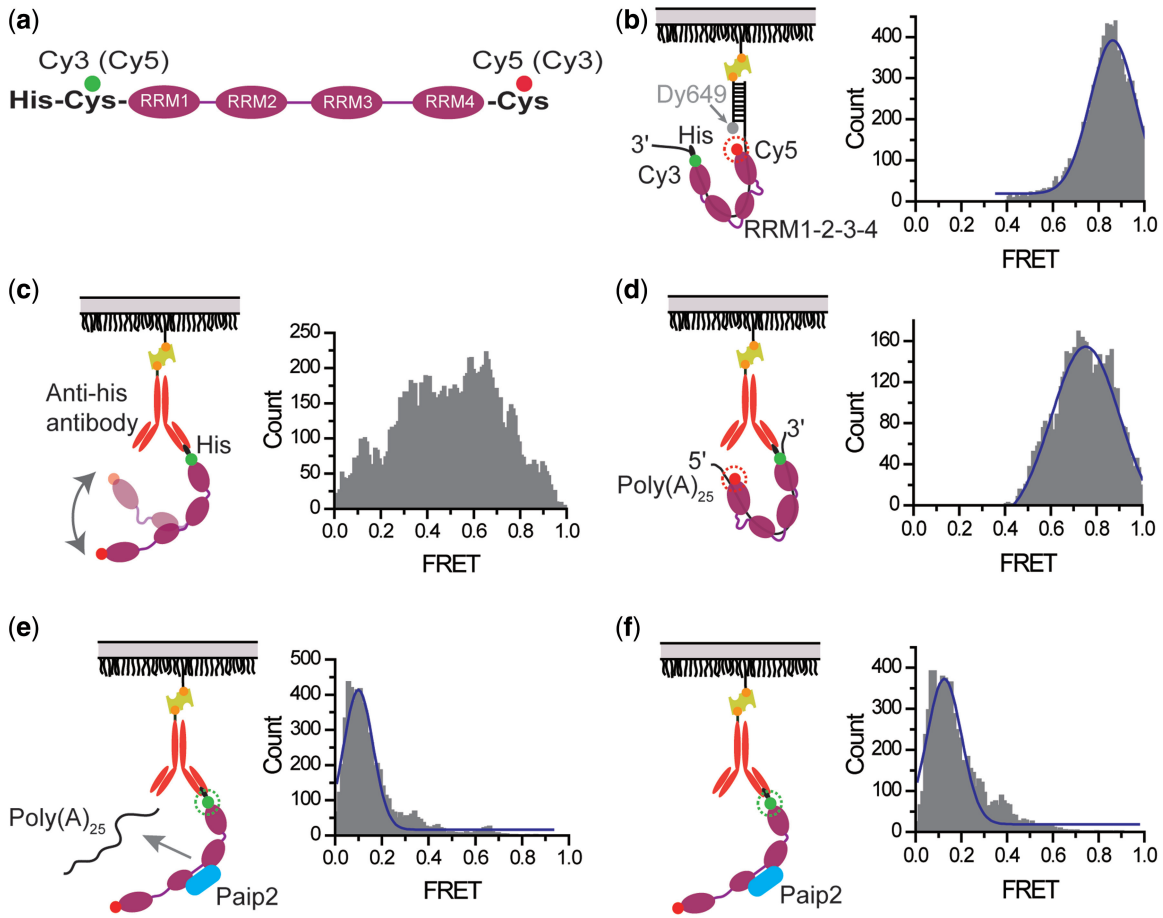

Figure 5. His-tagged RRM1-2-3-4 is immobilized on the flow chamber surface coated with an anti-His antibody. (**a**) Mutant RRM1-2-3-4 was labeled with a donor Cy3 and an acceptor Cy5. (**b**) Histogram of the FRET efficiency observed when fluorescently labeled RRM1-2-3-4 was bound to poly(A)$_{25}$ (N = 123). (**c**) A broad distribution of FRET efficiency was observed when RRM1-2-3-4 was immobilized on the flow chamber surface by the anti-His antibody (N = 217). (**d**) The broad distribution of FRET efficiency shifted to a high FRET efficiency in the presence of poly(A)$_{25}$ RNA (N = 103). (**e**) The FRET distribution of poly(A)$_{25}$ pre-assembled with RRM1-2-3-4 in the presence of Paip2 (N = 102). (**f**) When RRM1-2-3-4 was bound to Paip2, the FRET distribution was found to be nearly identical to the distribution shown in (**e**) (N = 114).

a complex with PABP during or immediately after inducing the dissociation of poly(A) from PABP. The resulting FRET distribution of RRM1-2-3-4 bound to Paip2 showed a peak with a low FRET efficiency of 0.10 ± 0.06 (N = 102; Figure 5e). To confirm, the conformational change of RRM1-2-3-4 in response to Paip2 binding, we investigated the FRET distribution of RRM1-2-3-4 in the absence of poly(A) RNA but in the presence of 500 nM Paip2 (Supplementary Figure S11d). The histogram of the FRET efficiency obtained from 114 RRM1-2-3-4 molecules is similar to that shown in Figure 5e (0.13 ± 0.08; Figure 5f). Moreover, we directly monitored the dissociation of poly(A) from PABP induced by Paip2 binding through observation of FRET signals from a FRET pair-labeled poly(A)$_{25}$ that is bound to PABP immobilized on the surface (Supplementary Figure S12a). In most traces, the donor–acceptor signals abruptly disappeared at 27.5 ± 7.7 s after the injection of Paip2 without detectable intermediate FRET in 50-ms time resolution (Supplementary Figure S12b and c). However, 22% events displayed intermediate FRET states before the loss of FRET, which indicates that Paip2 can bind to poly(A)-bound PABP until the conformation of PABP is completely rearranged. Taken as a whole, these results clearly show that the binding of Paip2 to RRM2-3 occurs concomitantly with the dissociation of poly(A) from the RRMs and that Paip2 linearly rearranges RRM2 and RRM3, whose linker was bent by poly(A) binding.

Paip2 directly interferes with the bent conformation of PABP

To further explore how Paip2 dissociates PABP from poly(A), we investigated the interaction between PABP and another PABP-interacting protein, Paip1, in the presence of poly(A) RNA. Paip1 physically interacting with RRM1-2 and PABC with a 1:1 stoichiometry (15,17) helps to stabilize the closed-loop formation of mRNA with other initiation factor, which differs from the 2:1 stoichiometry for the Paip2-PABP interaction (13) (Figure 6a). On the basis of the competition between Paip1 and Paip2 for PABP binding due to the common binding motifs (RRM2 and PABC) of Paip1 and Paip2 (18), we performed a single-molecule

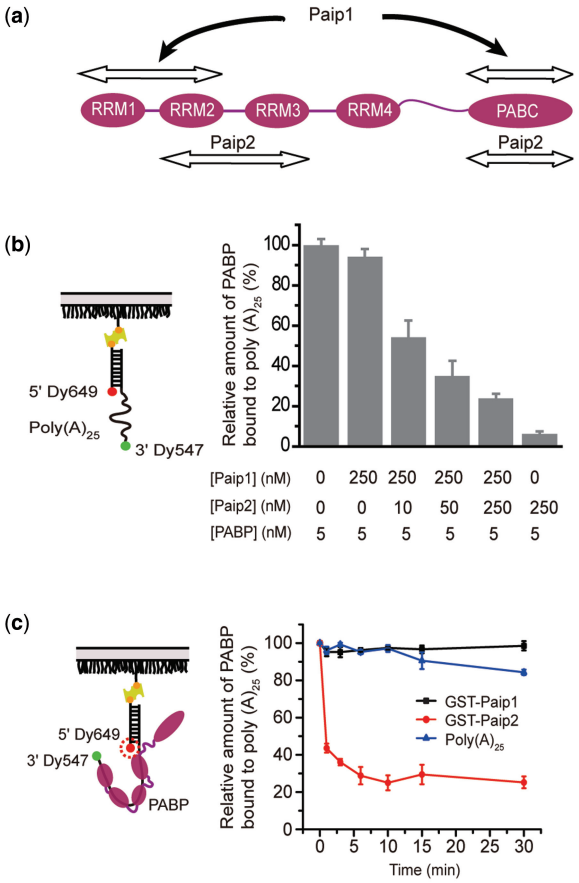

Figure 6. Paip2 does not interrupt the RNA-binding interface of PABP. (**a**) The Paip1 and Paip2 interaction sites in PABP. (**b**) The competition between Paip1 and Paip2 for PABP binding. The relative amounts of PABP bound to poly(A)$_{25}$ are shown by setting the amount of PABP bound to poly(A) without either Paip1 or Paip2 to 100% (0 nM, $N = 173$; 10 nM, $N = 135$; 50 nM, $N = 142$; 250 nM, $N = 151$). Paip1 did not interrupt the binding of PABP to poly(A), but Paip2 inhibited this binding. (**c**) Dissociation profiles of PABP from the PABP-poly(A)$_{25}$ complex over time by the addition of Paip1, Paip2 or poly(A)$_{25}$. The number of poly(A)$_{25}$ molecules in all data points was more than $N = 200$.

competition experiment of Paip1 and Paip2 on PABP binding to poly(A)$_{25}$ (Figure 6b). In this competition assay, the concentration of Paip2 increased with a fixed concentration of Paip1 (250 nM) and the template PABP was held constant at 5 nM. We confirmed the recombinant Paip1 was functional for PABP binding (Supplementary Figure S13). The number of poly(A)$_{25}$ molecules at the high FRET state gradually decreased as the increase of Paip2 from 0 to 250 nM (Figure 6b). The number of poly(A)$_{25}$ bound to PABP in the presence of Paip1 (no Paip2) was nearly identical to that in the absence of both Paip1 and Paip2 (second column in Figure 6b; $N = 570$), which indicates that Paip1 does not interrupt the binding of poly(A) by PABP. However, Paip2 ($N = 178$) prevented the binding of PABP to poly(A) efficiently (95%; sixth column in Figure 6b), and this prevention efficiency was partially nullified in the presence of equimolar amounts of Paip1 (78%). These results confirm previous reports showing that Paip1 does not affect the binding of poly(A) by PABP but competes with Paip2 for binding to PABP (18). Taken together, these results indicate that Paip2 inhibits the binding of PABP to poly(A) without associating with the RNA-binding interface of PABP because Paip1, which competes for the same RRM2 of PABP with Paip2, does not disrupt the poly(A) binding of PABP.

We also confirmed that Paip1 rarely dissociated PABP from poly(A) in contrast to Paip2 (Figure 6c). Interestingly, the number of PABP proteins bound to poly(A) decreased by ~15% in 30 min by poly(A) competition, which suggests that excess poly(A) molecules in solution competed with poly(A) bound to PABP weakly. Although PABP forms a extremely stable conformation with poly(A), it was previously reported that excess free poly(A) in solution can replace poly(A) bound to yeast PABP through the transient loosening of RRM binding to poly(A) (24).

DISCUSSION

On the basis of the co-crystal structure of RRM1-2 with poly(A) and the homology between RRM1-2 and RRM3-4, it has been speculated that each RRM in full-length PABP bound to poly(A) is linearly arranged along the poly(A) RNA (3,37). However, surprisingly, our single-molecule results suggest that RRM1-2-3-4 undergoes a conformational change on binding to poly(A) from a fluctuating conformation in the absence of poly(A): the region between RRM2 and RRM3 primarily contributes to the bent conformation of RRM1-2-3-4 and the region between RRM3 and RRM4 bends slightly, but RRM1-2 is aligned straight 3′ to 5′ along the poly(A) (Figures 1–3). The bent conformation of PABP allows the direct interaction of C-terminal domains of two PABP molecules with the same directionality, which is not be possible if PABP is aligned on poly(A) in a linear conformation (37). The specific arrangement of RRMs on poly(A) provides a new insight for interactions of multiple PABP molecules on the poly(A) (Figure 3c and d). According to the low FRET efficiency ($E \sim 0.1$) of RRM1-2-3-4 bound to Paip2 and the crystallographic length of RRM1-2 (4.7 nm) (3), the broad FRET distribution for RRM1-2-3-4 in Figure 5c, which is mostly populated between $E \sim 0.4$ and $E \sim 0.7$, suggests that poly(A)-free PABP fluctuates among various bent conformations (Supplementary Figure S11). The fluctuating bent conformation of RRM1-2-3-4 may be rapidly stabilized by the binding of poly(A) (Figure 2a; Supplementary Figure S11b). The events showing the transient intermediate FRET states before the high FRET significantly decreased at the longer poly(A)$_{37}$ (Supplementary Figure S3). This suggests that the fast transition to the bent conformation is more probable when poly(A) is long enough to be occupied simultaneously by all RRMs of PABP. However, to further understand the molecular mechanism of the bent conformation of PABP by poly(A) binding, it is proposed that the role of the flexible linkers between RRMs and the interactions of RRMs and poly(A)

should be investigated using NMR, X-ray structure or a faster time resolution single-molecule techniques (38).

The long dwell time of PABP on poly(A) and its high concentration *in vivo* (~4 μM) (39) necessitate a mechanism for regulating the binding of PABP to poly(A), so that PABP can function as a translational regulator. It has been recognized that Paip2 is responsible for maintaining PABP homeostasis through their physical interactions *in vivo* (40,41). There are two possible mechanisms for the dissociation of poly(A) from PABP via its interaction with Paip2: (i) a transient fraying of the PABP-poly(A) complex allows for the invasion of the 14.5 kDa Paip2 to the poly(A)-binding interfaces and (ii) Paip2 disrupts the binding of poly(A) to PABP by inducing a conformational change in PABP. We favor the latter mechanism because Paip1, which overlaps a Paip2-binding RRM of PABP, does not interrupt the binding of PABP to poly(A) (Figure 6). Although poly(A) bound to PABP can be replaced by poly(A) in solution, this replacement occurs slowly and its probability is extremely low (Figure 6c). Therefore, it is unlikely that Paip2 binds to the RNA-binding interface of PABP during the transient dissociation of the RRMs from poly(A), considering the fast kinetics of the dissociation of PABP from poly(A) mediated by Paip2 (Figure 6c). Moreover, the RRM2 and RRM3 domains of PABP are known to participate in the interaction with Paip2, and Paip2 displays a much stronger interaction with the RRM2-3 fragment than with the individual RRM2 or RRM3 domains (13). We speculate that the junction of these RRM2 and RRM3, which is sharply bent on binding to poly(A), is unbent by the binding of Paip2. The extended form of PABP may lead to weak binding of poly(A).

Interestingly, the binding affinity of Paip2 to poly(A)-bound PABP was 10-fold smaller than that of Paip2 to poly(A)-free PABP [Figure 4d and Karim *et al* (19)]. We suspect that the seemingly slow binding of Paip2 to PABP associated with poly(A) is attributable to the unfavorable conformation of PABP associated with poly(A) for the interaction with Paip2 because ~20% of the dissociation events of PABP from poly(A) that result from Paip2 binding displayed an intermediate state of dissociation. The intermediate state would be a ternary complex composed of PABP partially associated with both Paip2 and poly(A). We also speculate that the faster kinetics of Paip2 binding to PABP in the absence of poly(A) results from the flexibility of PABP, as flexible random-coil polymers can have a faster binding rate of target molecules than polymers with a rigid globule conformation (42). Considering the association rates of poly(A) to PABP ($0.78 \times 10^7 M^{-1}\ s^{-1}$; Supplementary Figure S14), Paip2 to poly(A)-bound PABP ($1.53 \times 10^5 M^{-1}\ s^{-1}$; Figure 4d), and Paip2 to PABP ($1.9 \times 10^6 M^{-1}\ s^{-1}$) (19), the direct interaction between Paip2 and PABP, rather than the interruption of PABP bound to 3′ poly(A) tail, is more likely to occur if they exist in equimolar amounts. However, the interplay between PABP and Paip2 would depend on the concentrations and availabilities of the poly(A) RNA and PABP and Paip2 protein levels in the cell.

SUPPLEMENTARY DATA

Supplementary data are available at NAR Online

ACKNOWLEDGEMENTS

The authors thank Changbong Hyeon for the helpful discussion.

FUNDING

National Research Foundation of Korea (NRF) grant funded by the Korea government (MEST) [2010-0019706, No. 2011-0013901 and No. 313-2008-2-C00364]; and World Class University (WCU) program through NRF funded by MEST [R31-10105]. Funding for open access charge: School of Interdisciplinary Bioscience & Bioengineering, POSTECH.

Conflict of interest statement. None declared.

REFERENCES

1. Mangus,D.A., Evans,M.C. and Jacobson,A. (2003) Poly(A)-binding proteins: multifunctional scaffolds for the post-transcriptional control of gene expression. *Genome Biol.*, **4**, 223.
2. Smith,R.W. and Gray,N.K. (2010) Poly(A)-binding protein (PABP): a common viral target. *Biochem. J.*, **426**, 1–12.
3. Deo,R.C., Bonanno,J.B., Sonenberg,N. and Burley,S.K. (1999) Recognition of polyadenylate RNA by the poly(A)-binding protein. *Cell*, **98**, 835–845.
4. Handa,N., Nureki,O., Kurimoto,K., Kim,I., Sakamoto,H., Shimura,Y., Muto,Y. and Yokoyama,S. (1999) Structural basis for recognition of the tra mRNA precursor by the Sex-lethal protein. *Nature*, **398**, 579–585.
5. Wang,X. and Tanaka Hall,T.M. (2001) Structural basis for recognition of AU-rich element RNA by the HuD protein. *Nat. Struct. Biol.*, **8**, 141–145.
6. Finger,L.D., Trantirek,L., Johansson,C. and Feigon,J. (2003) Solution structures of stem-loop RNAs that bind to the two N-terminal RNA-binding domains of nucleolin. *Nucleic Acids Res.*, **31**, 6461–6472.
7. Auweter,S.D. and Allain,F.H. (2008) Structure-function relationships of the polypyrimidine tract binding protein. *Cell Mol. Life Sci.*, **65**, 516–527.
8. Oberstrass,F.C., Auweter,S.D., Erat,M., Hargous,Y., Henning,A., Wenter,P., Reymond,L., Amir-Ahmady,B., Pitsch,S., Black,D.L. *et al.* (2005) Structure of PTB bound to RNA: specific binding and implications for splicing regulation. *Science*, **309**, 2054–2057.
9. Jackson,R.J., Hellen,C.U. and Pestova,T.V. (2010) The mechanism of eukaryotic translation initiation and principles of its regulation. *Nat. Rev. Mol. Cell Biol.*, **11**, 113–127.
10. Wells,S.E., Hillner,P.E., Vale,R.D. and Sachs,A.B. (1998) Circularization of mRNA by eukaryotic translation initiation factors. *Mol. Cell*, **2**, 135–140.
11. Kahvejian,A., Svitkin,Y.V., Sukarieh,R., M'Boutchou,M.N. and Sonenberg,N. (2005) Mammalian poly(A)-binding protein is a eukaryotic translation initiation factor, which acts via multiple mechanisms. *Genes Dev.*, **19**, 104–113.
12. Wilkie,G.S., Dickson,K.S. and Gray,N.K. (2003) Regulation of mRNA translation by 5′- and 3′-UTR-binding factors. *Trends Biochem. Sci.*, **28**, 182–188.
13. Khaleghpour,K., Kahvejian,A., De Crescenzo,G., Roy,G., Svitkin,Y.V., Imataka,H., O'Connor-McCourt,M. and Sonenberg,N. (2001) Dual interactions of the translational repressor Paip2 with poly(A) binding protein. *Mol. Cell Biol.*, **21**, 5200–5213.
14. Hoshino,S., Imai,M., Kobayashi,T., Uchida,N. and Katada,T. (1999) The eukaryotic polypeptide chain releasing factor (eRF3/

GSPT) carrying the translation termination signal to the 3′-Poly(A) tail of mRNA. Direct association of erf3/GSPT with polyadenylate-binding protein. *J. Biol. Chem.*, **274**, 16677–16680.
15. Roy,G., De Crescenzo,G., Khaleghpour,K., Kahvejian,A., O'Connor-McCourt,M. and Sonenberg,N. (2002) Paip1 interacts with poly(A) binding protein through two independent binding motifs. *Mol. Cell Biol.*, **22**, 3769–3782.
16. Gray,N.K., Coller,J.M., Dickson,K.S. and Wickens,M. (2000) Multiple portions of poly(A)-binding protein stimulate translation *in vivo*. *EMBO J.*, **19**, 4723–4733.
17. Craig,A.W., Haghighat,A., Yu,A.T. and Sonenberg,N. (1998) Interaction of polyadenylate-binding protein with the eIF4G homologue PAIP enhances translation. *Nature*, **392**, 520–523.
18. Khaleghpour,K., Svitkin,Y.V., Craig,A.W., DeMaria,C.T., Deo,R.C., Burley,S.K. and Sonenberg,N. (2001) Translational repression by a novel partner of human poly(A) binding protein, Paip2. *Mol. Cell*, **7**, 205–216.
19. Karim,M.M., Svitkin,Y.V., Kahvejian,A., De Crescenzo,G., Costa-Mattioli,M. and Sonenberg,N. (2006) A mechanism of translational repression by competition of Paip2 with eIF4G for poly(A) binding protein (PABP) binding. *Proc. Natl Acad. Sci. USA*, **103**, 9494–9499.
20. Sladic,R.T., Lagnado,C.A., Bagley,C.J. and Goodall,G.J. (2004) Human PABP binds AU-rich RNA via RNA-binding domains 3 and 4. *Eur. J. Biochem.*, **271**, 450–457.
21. Jeong,C., Cho,W.K., Song,K.M., Cook,C., Yoon,T.Y., Ban,C., Fishel,R. and Lee,J.B. (2011) MutS switches between two fundamentally distinct clamps during mismatch repair. *Nat. Struct. Mol. Biol.*, **18**, 379–385.
22. Park,J., Jeon,Y., In,D., Fishel,R., Ban,C. and Lee,J.B. (2010) Single-molecule analysis reveals the kinetics and physiological relevance of MutL-ssDNA binding. *PLoS One*, **5**, e15496.
23. Chung,S.H. and Kennedy,R.A. (1991) Forward-backward non-linear filtering technique for extracting small biological signals from noise. *J. Neurosci. Methods*, **40**, 71–86.
24. Sachs,A.B., Davis,R.W. and Kornberg,R.D. (1987) A single domain of yeast poly(A)-binding protein is necessary and sufficient for RNA binding and cell viability. *Mol. Cell Biol.*, **7**, 3268–3276.
25. Baer,B.W. and Kornberg,R.D. (1983) The protein responsible for the repeating structure of cytoplasmic poly(A)-ribonucleoprotein. *J. Cell Biol.*, **96**, 717–721.
26. Baer,B.W. and Kornberg,R.D. (1980) Repeating structure of cytoplasmic poly(A)-ribonucleoprotein. *Proc. Natl Acad. Sci. USA*, **77**, 1890–1892.
27. Saenger,W., Riecke,J. and Suck,D. (1975) A structural model for the polyadenylic acid single helix. *J. Mol. Biol.*, **93**, 529–534.
28. Lamichhane,R., Daubner,G.M., Thomas-Crusells,J., Auweter,S.D., Manatschal,C., Austin,K.S., Valniuk,O., Allain,F.H. and Rueda,D. (2010) RNA looping by PTB: Evidence using FRET and NMR spectroscopy for a role in splicing repression. *Proc. Natl Acad. Sci. USA*, **107**, 4105–4110.
29. Melo,E.O., Dhalia,R., Martins de Sa,C., Standart,N. and de Melo Neto,O.P. (2003) Identification of a C-terminal poly(A)-binding protein (PABP)-PABP interaction domain: role in cooperative binding to poly (A) and efficient cap distal translational repression. *J. Biol. Chem.*, **278**, 46357–46368.
30. Kuhn,U. and Wahle,E. (2004) Structure and function of poly(A) binding proteins. *Biochim. Biophys. Acta*, **1678**, 67–84.
31. Kozlov,G., Trempe,J.F., Khaleghpour,K., Kahvejian,A., Ekiel,I. and Gehring,K. (2001) Structure and function of the C-terminal PABC domain of human poly(A)-binding protein. *Proc. Natl Acad. Sci. USA*, **98**, 4409–4413.
32. Deo,R.C., Sonenberg,N. and Burley,S.K. (2001) X-ray structure of the human hyperplastic discs protein: an ortholog of the C-terminal domain of poly(A)-binding protein. *Proc. Natl Acad. Sci. USA*, **98**, 4414–4419.
33. Kim,S.E., Lee,I.B. and Hong,S.C. (2012) The effect of the oxygen scavenging system on the pH of buffered sample solutions: in the context of single-molecule fluorescence measurements. *Bull Korean Chem. Soc.*, **33**, 958–962.
34. Lamboy,J.A., Kim,H., Lee,K.S., Ha,T. and Komives,E.A. (2011) Visualization of the nanospring dynamics of the IkappaBalpha ankyrin repeat domain in real time. *Proc. Natl Acad. Sci. USA*, **108**, 10178–10183.
35. Yeom,K.H., Heo,I., Lee,J., Hohng,S., Kim,V.N. and Joo,C. (2011) Single-molecule approach to immunoprecipitated protein complexes: insights into miRNA uridylation. *EMBO Rep.*, **12**, 690–696.
36. Jain,A., Liu,R., Ramani,B., Arauz,E., Ishitsuka,Y., Ragunathan,K., Park,J., Chen,J., Xiang,Y.K. and Ha,T. (2011) Probing cellular protein complexes using single-molecule pull-down. *Nature*, **473**, 484–488.
37. Lin,J., Fabian,M., Sonenberg,N. and Meller,A. (2012) Nanopore detachment kinetics of poly(A) binding proteins from RNA molecules reveals the critical role of C-terminus interactions. *Biophys. J.*, **102**, 1427–1434.
38. Daubner,G.M., Clery,A. and Allain,F.H. (2013) RRM-RNA recognition: NMR or crystallography. and new findings. *Curr. Opin. Struct. Biol.*, **23**, 100–108.
39. Gorlach,M., Burd,C.G. and Dreyfuss,G. (1994) The mRNA poly(A)-binding protein: localization, abundance, and RNA-binding specificity. *Exp. Cell Res.*, **211**, 400–407.
40. Yoshida,M., Yoshida,K., Kozlov,G., Lim,N.S., De Crescenzo,G., Pang,Z., Berlanga,J.J., Kahvejian,A., Gehring,K., Wing,S.S. *et al.* (2006) Poly(A) binding protein (PABP) homeostasis is mediated by the stability of its inhibitor, Paip2. *EMBO J.*, **25**, 1934–1944.
41. Yanagiya,A., Delbes,G., Svitkin,Y.V., Robaire,B. and Sonenberg,N. (2010) The poly(A)-binding protein partner Paip2a controls translation during late spermiogenesis in mice. *J. Clin. Invest.*, **120**, 3389–3400.
42. Hoshino,Y., Nakamoto,M. and Miura,Y. (2012) Control of protein-binding kinetics on synthetic polymer nanoparticles by tuning flexibility and inducing conformation changes of polymer chains. *J. Am. Chem. Soc.*, **134**, 15209–15212.